Dyes and Pigments 117 (2015) 141–148

Contents lists available at ScienceDirect

Dyes and Pigments

journal homepage: www.elsevier.com/locate/dyepig

Thermally activated delayed fluorescence of *N*-phenylcarbazole and triphenylamine functionalised tris(aryl)triazines

Bin Huang [a, b], Zhihui Yin [b], Xinxin Ban [a], Wei Jiang [a, *], Yu Dai [b], Junya Zhang [b], Yuanyuan Liu [b], Yaping Yang [b], Yueming Sun [a, *]

[a] School of Chemistry and Chemical Engineering, Southeast University, Nanjing, Jiangsu 211189, PR China
[b] Department of Chemical and Pharmaceutical Engineering of Southeast University Chengxian College, Nanjing, Jiangsu 210088, PR China

ARTICLE INFO

Article history:
Received 8 January 2015
Received in revised form
16 February 2015
Accepted 17 February 2015
Available online 25 February 2015

Keywords:
Carbazole
Triazine
Benzonitrile
Triphenylamine
TADF
Bipolar

ABSTRACT

N–phenyl carbazole and triphenylamine functionalized tris(aryl)triazines, as well as the corresponding mononers, have been synthesized by Suzuki cross–coupling reactions. The electronic, photophysical and electrochemical properties of these materials can be effectively tuned by manipulation of the constitution of acceptor and donor units. *N*–phenyl carbazole and triphenylamine functionalized 2,4,6–trisphenyl–1,3,5–triazines exhibit small energy gaps between the singlet and triplet (0.24 eV and 0.18 eV), and offer potential for application as thermally activated delayed fluorescence materials. The results are supported by time–dependent density functional theory calculations, delayed and time-resolved fluorescence data.

1. Introduction

In recent years, tremendous efforts have been made in the development of materials for phosphorescent organic light emitting diodes (PHOLEDs) due to 100% theoretical internal efficiency [1–6]. Phosphorescent host materials and phosphors are indispensable to obtain high–efficiency PHOLEDs. However, traditional phosphors based on precious transition metals such as Ir(?), Pt(?), or Os(?) are rather expensive. The development of cheaper alternatives has attracted more and more attention [7,8]. One promising solution for this issue is the use of thermally activated delayed fluorescence (TADF) materials because they have the potential to substitute the phosphors for cost–effective and high–efficiency environmentally OLEDs [9–13].

For a TADF molecule, a small energy gap between the singlet and triplet (ΔE_{ST}) is required to promote reverse intersystem crossing (ISC) [9]. To achieve efficient TADF, the most probable way is via bipolar compounds based on intramolecular charge transfer (ICT) within systems containing donor and acceptor moieties. In an ICT based compound, the highest occupied molecule orbital (HOMO) and lowest unoccupied molecule orbital (LUMO) would be localized at the donor and acceptor moieties, respectively. Thus, effective separation of HOMO and LUMO leads to a small ΔE_{ST}. Enormous attempts have been made in the development of materials with small ΔE_{ST} values. Various TADF materials based on donor substituted cyanobenzene [9,14,15], triazine [16–25], sulfone [26–28], benzophenone [29], spirofluorene [30], oxadiazole and triazole [31] have been designed and applied to realize high–performance OLEDs.

Recently, our group reported a bipolar host composed of electron–transporting 2,4,6–trisphenyltriazine and hole–transporting *N*–phenylcarbazole, namely 2,4,6–tris(3–((9–phenyl)carbazol–3–yl)phenyl)triazine (**3a**) [32]. Utilizing **3a** as host material, highly efficient solution–processed single layer green PhOLED has been achieved. Density functional theory (DFT) has revealed that the LUMO level of **3a** is localized predominantly on the 2,4,6–trisphenyl–1,3,5–triazine unit while the HOMO level is distributed over the outer layer *N*–phenylcarbazole unit with a limited HOMO–LUMO overlap. The low HOMO–LUMO overlap leads to a small ΔE_{ST} of 0.24 eV. Inspired by the results, we have designed triphenylamine substituted 2,4,6–trisphenyl–1,3,5–triazine (**3b**) and decreased the ΔE_{ST} to 0.18 eV. To verify the TADF behavior of **3a**

* Corresponding authors. Tel./fax: +86 25 52090621.
E-mail address: 101011462@seu.edu.cn (W. Jiang).

http://dx.doi.org/10.1016/j.dyepig.2015.02.014
0143-7208/

and **3b**, we present a detailed study of photophysical characteristics including fluorescence solvatochromical effects, time-resolved fluorescence and phosphorescence, delayed fluorescence lifetime, and time–dependent density functional theory (TD–DFT). To reveal the importance of molecular configuration for giving effective TADF, *N*–phenylcarbazole and triphenylamine substituted benzonitriles (**2a**, **2b**) as the corresponding monomers of **3a** and **3b** have been prepared for comparison in this paper.

2. Experimental

2.1. General

DFT calculations of these compounds were performed using the Gaussian 09 program package [33]. The calculations were optimized at the B3LYP/6–31G(d) level of theory. The molecular orbitals were visualized using Gaussview. To investigate the properties of the excited states of these compounds, we performed quantum chemical calculations of the low–lying excited states of these compounds using TD–DFT. The ten lowest singlet and triplet excited states were calculated by the TD–DFT method at their optimized ground–state geometries using the same functional and basis set [12].

All materials and reagents were purchased from commercial sources and used without further purification. IR spectra were recorded on a 5DX-FT-2 spectrophotometer using KBr pellets. ^{1}H NMR and ^{13}C NMR spectra were recorded on a Bruker ARX300 NMR spectrometer at room temperature. Elemental analyses were performed on an Elementar Vario EL CHN elemental analyzer. UV–vis absorption spectra and fluorescence spectra were recorded on a spectrophotometer (Agilent 8453) and a fluorospectrophotometer (Jobin Yvon, Fluoromax–3), respectively. The transient photoluminescence decay characteristics and time-resolved fluorescence were recorded using a spectrofluorometer (Floromax-4, Horiba). The fast decay component was recorded with a 350 nm LED excitation source, while the slow decay component was recorded with a flash lamp source. Cyclic voltammetry (CV) measurements was carried out on a Princeton Applied Research potentiostat/galvanostat model 283 voltammetric analyzer in CH_2Cl_2 solutions (10^{-3} M) at a scan rate of 100 mV s^{-1} with a conventional three–electrode configuration consisting of platinum plate working electrode, a silver wire pseudo–reference electrode, and a platinum wire counter electrode. The supporting electrolyte was tetrabutylammonium hexafluorophosphate ($TBAPF_6$, 0.1 M) and ferrocene was selected as the internal standard. The solutions were bubbled with a constant nitrogen flow for 10 min before measurements.

2.1.1. X-ray crystallography

X-ray crystallographic analysis of **2b** was performed on a Nonius CAD-4 single-crystal diffractometer by using MoK_α radiation ($\lambda = 0.71073$ Å) with an $\omega/2\theta$ scan mode at 293 K. The structure was solved by direct methods and refined by full-matrix least-squares procedures on F^2 using SHELXL-97 program. All non-hydrogen atoms were refined anisotropically, and the hydrogen atoms were introduced at calculated positions. The isotropic temperature factors were fixed to 1.2 times (1.5 times for CH_3 groups) the equivalent isotropic displacement parameters of the C-atom which the H-atom was attached to. Drawings were produced using Diamond 3.0 and Mercury 1.4.1 software. Crystallographic data for the structure in this paper has been deposited with the Cambridge Crystallographic Data Centre as supplemental publications.

CCDC 994818 for **2b**. The data can be obtained free of charge from the Cambridge Crystallographic Data Centre via www.ccdc.cam.ac.uk/datarequest/cif.

2.2. Synthesis

2.2.1. Synthesis of 3–((9–phenyl)carbazol–3–yl)–benzonitrile (*2a*)

To a solution of 3–bromobenzonitrile (0.546 g, 3.0 mmol) and *N*–phenyl–3–(4,4,5,5– tetramethyl–1,3,2–dioxaborolane–2–yl)–6*H*–carbazole (**1a**, 1.107 g, 3.0 mmol) in toluene (20 mL) and ethanol (4 mL) was added aqueous K_2CO_3 solution (2.0 M, 2 mL). The reaction mixture was then purged with nitrogen for 10 min before adding tetrakis(triphenylphosphine)palladium(0) (0.055 g, 0.048 mmol). The reaction mixture was heated under reflux for 24 h under nitrogen. The resulting mixture was cooled to room temperature and then poured into water and extracted with CH_2Cl_2 (3 × 20 mL). The combined organic phase was washed with saturated aqueous NaCl solution (2 × 10 mL) and dried with anhydrous Na_2SO_4. After removal of the solvent by rotary evaporation, the residue was purified by silica gel column chromatography to afford **2a** as a white solid. Yield: 73.6%. Mp: 117–119 °C. IR (KBr, cm^{-1}):3057, 2225, 1626, 1597, 1501, 1472, 1455, 1402, 1361, 1232. ^{1}H NMR (300 MHz, $CDCl_3$) δ(ppm): 8.35 (s, 1H), 8.24–8.21 (d, J = 7.5 Hz, 1H), 8.02 (s, 1H), 7.98–7.93 (d, J = 7.5 Hz, 1H), 7.69–7.36 (m, 12H). ^{13}C NMR (75 MHz, $CDCl_3$) δ(ppm):110.46, 110.74, 113.25, 119.24, 119.48, 120.75, 120.79, 123.57, 124.44, 125.44, 126.88, 127.39, 128.10, 129.92, 130.25, 130.37, 131.06, 131.22, 131.91, 137.73, 141.19, 141.82, 143.50. Anal. Calcd. for $C_{25}H_{16}N_2$ (%): C, 87.18; H, 4.68; N, 8.13. Found: C, 87.28; H, 4.72; N, 8.19. MS (MALDI-TOF) [m/z]:Calcd for $C_{25}H_{16}N_2$, 344.41; found, 344.3834.

2.2.2. Synthesis of N,N–diphenyl–(1,1′–biphenyl)–3′–cyano-4–amine (*2b*)

A procedure similar to that used for **2a** was followed but with *N*,*N*–diphenyl–4–(4,4,5,5–tetramethyl–1,3,2–dioxaborolan–2–-yl)aniline (**1b**) instead of **1a**. Yield: 62.5%. Mp: 122–124 °C. IR (KBr, cm^{-1}): 3005, 2229, 1588, 1514, 1482, 1432, 1401, 1330, 1276. ^{1}H NMR (300 MHz, $CDCl_3$) δ(ppm): 7.83 (s, 1H), 7.79–7.77 (d, J = 7.8 Hz, 1H), 7.59–7.48 (m, 2H), 7.44–7.41 (d, J = 8.7 Hz, 2H), 7.32–7.26 (m, 4H), 7.16–7.04 (m, 8H). ^{13}C NMR (75 MHz, $CDCl_3$) δ(ppm):113.29, 119.33, 123.26, 123.70, 123.85, 124.75, 125.19, 128.11, 129.45, 129.82, 129.96, 130.45, 130.37, 131.21, 132.45, 142.25, 147.73, 148.66. Anal. Calcd. for $C_{25}H_{18}N_2$ (%): C, 86.68; H, 5.24; N, 8.09. Found: C, 86.74; H, 5.22; N, 8.13. MS (MALDI-TOF)[m/z]:Calcd for $C_{25}H_{18}N_2$, 346.42; found, 346.2814.

2.2.3. Synthesis of 3′,3‴,3‴″–(1,3,5–triazine–2,4,6–triyl) tris(N,N–diphenyl–(1,1′–biphenyl)–4–amine) (*3b*)

To a solution of 2,4,6–tris(3–bromophenyl)triazine (**1c**, 0.546 g, 1.0 mmol) and **1b** (1.113 g, 3.0 mmol) in toluene (20 mL) and ethanol (4 mL) was added 2 mL of 2.0 M aqueous Na_2CO_3 solution. The reaction mixture was then purged with nitrogen for ten minutes before adding tetrakis(triphenylphosphine)palladium(0) (0.055 g, 0.048 mmol). The reaction mixture was heated under reflux for 24 h under nitrogen. The resulting mixture was cooled to room temperature and then poured into water and extracted with CH_2Cl_2 (3 × 20 mL). The combined organic phase was washed with saturated aqueous NaCl solution (2 × 10 mL) and dried with anhydrous Na_2SO_4. After removal of the solvent by rotary evaporation, the residue was purified by silica gel column chromatography to afford **3b** as a yellow solid. Yield: 42.4%. Mp: 209–211 °C. IR (KBr, cm^{-1}): 3060, 3032, 1591, 1527, 1510, 1492, 1436, 1406, 1358, 1328, 1276. ^{1}H NMR(300 MHz, $CDCl_3$) δ(ppm): 9.00 (s, 3H), 8.77–8.74 (d, J = 7.5 Hz, 3H), 7.86–7.83 (d, J = 7.5 Hz, 3H), 7.67–7.64 (d, J = 8.1 Hz, 9H), 7.31–7.06 (m, 36H). ^{13}C NMR (75 MHz, $CDCl_3$) δ(ppm):123.44, 124.33, 124.88, 127.42, 127.92, 128.34, 129.48, 129.73, 131.12, 134.96, 137.12, 141.40, 147.90, 148.05, 172.03. Anal. Calcd. for $C_{75}H_{54}N_6$ (%): C, 86.68; H, 5.24; N, 8.09. Found: C, 86.74;

H, 5.21; N, 8.05. MS (MALDI-TOF) [m/z]: Calcd for $C_{75}H_{54}N_6$, 1038.44; found, 1038.3820.

3. Results and discussion

3.1. Synthesis and characterization

Scheme 1 shows the synthetic routes and structures of the four compounds. Firstly, **1a**, **1b** and **1c** were synthesized according to the literature procedures [34–36]. Subsequently, **2a**, **2b** and **3b** were prepared via Suzuki cross–coupling reactions with yields of 73.6%, 62.5% and 42.4%, respectively. Finally, the products were purified by column chromatography to give the pure products. IR, ^{1}H NMR, ^{13}C NMR, MS and elemental analysis were employed to confirm the chemical structures of the four compounds.

3.2. DFT calculations

DFT calculations were performed to gain insight into the geometric and electronic structures of the four compounds. Triplet and singlet excitation energies (vertical transition), oscillator strength (f), and transition configurations of the four compounds calculated by TD-DFT are listed in Table 1. The HOMOs, LUMOs of the four compounds are shown in Fig. 1. The dihedral angles between the donor groups and the adjacent phenyl rings of the four compounds are calculated to be 35°–37° in their optimized ground–state geometries. The HOMOs of **3a** and **3b** are delocalized over the outer *N*–phenylcarbazole and triphenylamine units, while their LUMOs are delocalized over the central 2,4,6–trisphenyl–1,3,5–triazine unit with small HOMO–LUMO overlaps, indicating that their HOMO–to–LUMO transitions have strong CT character [27]. The

Table 1
Triplet and singlet excitation energies (vertical transition), oscillator strength (f), and transition configurations of the four compounds calculated by TD-DFT at the B3LYP/6-31G(d).

Compound	Dihedral angle	State	E (eV)	f	Main configuration[a]		ΔE_{ST} (eV)
2a	37.91°	S1	3.76	0.097	H–L	0.70	0.75
		S2	3.91	0.021	H–L+1	0.64	
		T1	3.01	0.00	H–L	0.34	
		T2	3.25	0.00	H–L+1	0.44	
2b	35.69°	S1	3.36	0.243	H–L	0.70	0.62
		S2	3.65	0.338	H–L+1	0.70	
		T1	2.74	0.00	H–L	0.50	
		T2	3.22	0.00	H–L+1	0.58	
3a	37.45°	S1	3.19	0.0028	H–L+1	0.60	0.37
		S2	3.19	0.0099	H–L+1	0.35	
		T1	2.82	0.00	H–L	0.18	
		T2	2.90	0.00	H–L+1	0.38	
3b	35.92°	S1	2.82	0.0093	H–L	0.48	0.18
		S2	2.82	0.014	H–1–L+1	0.64	
		T1	2.64	0.00	H–L	0.17	
		T2	2.66	0.00	H–1–L+1	0.42	

[a] H→L represents the HOMO to LUMO transition. Excitation configurations with the highest contributions are presented, together with the corresponding transition symmetry and nature of the involved orbitals.

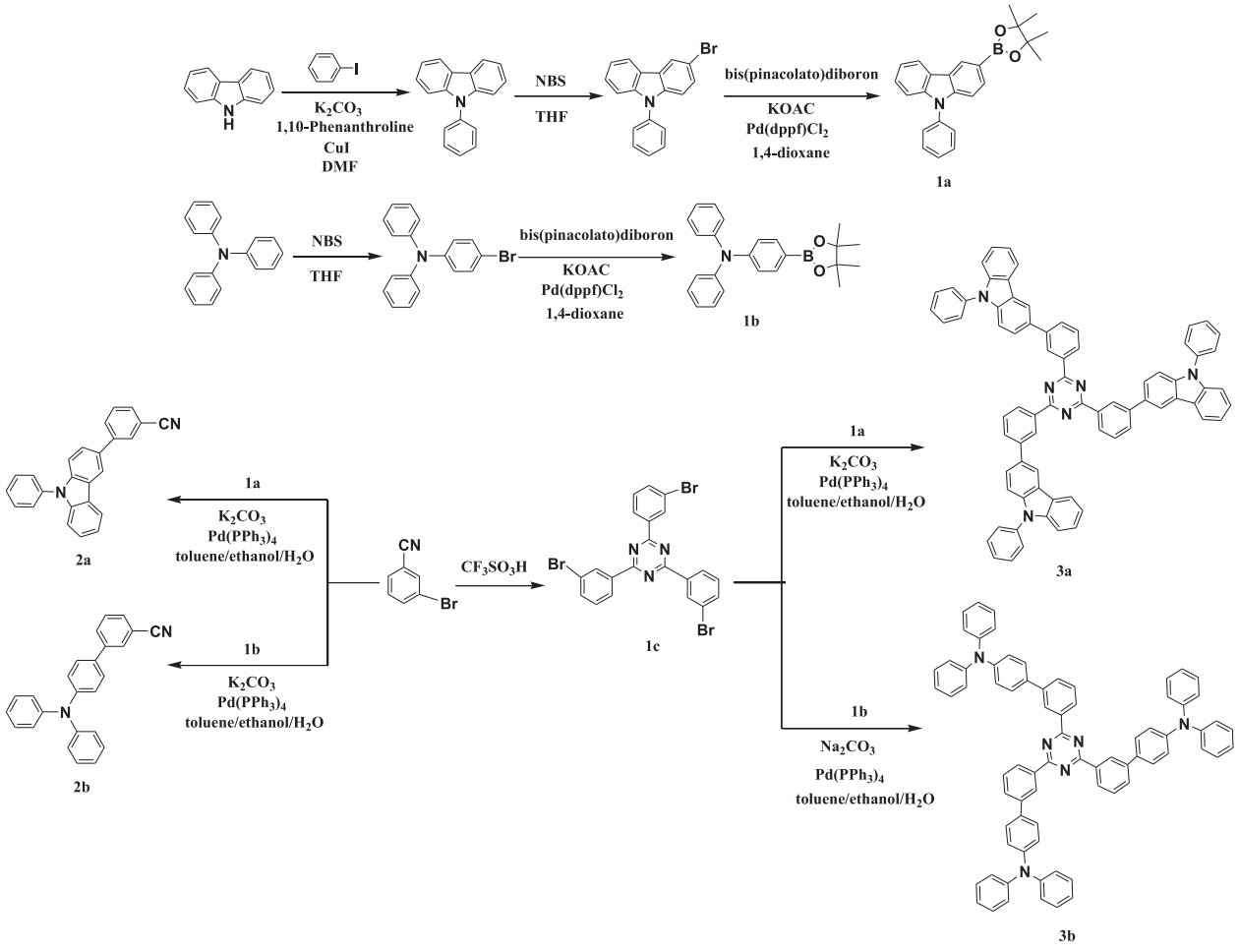

Scheme 1. Synthetic route to the target compounds.

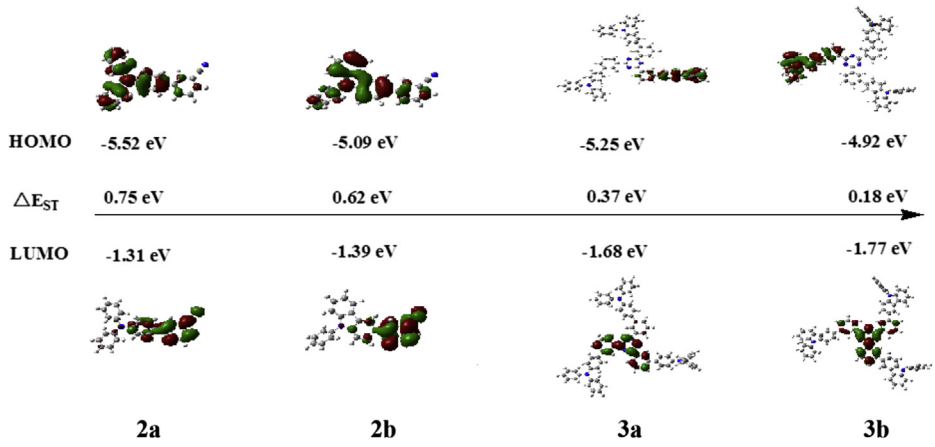

Fig. 1. Optimized geometries and calculated HOMO and LUMO density maps for the four compounds.

clear separation of HOMO and LUMO lead to a smaller ΔE_{ST} of **3b** (0.18 eV) than that of **3a** (0.37 eV), this may be attributed to the higher electron–donating ability of triphenylamine comparing to *N*–phenylcarbazole. The result is in agreement with the reported thioxanthone derivatives [37]. Among them, changing the donor from *N*–phenylcarbazole to triphenylamine group induces a decrease of ΔE_{ST}. Changing the acceptor from 2,4,6–trisphenyl–1,3,5–triazine to a benzonitrile, the HOMO–LUMO overlaps become larger, thus led to larger ΔE_{ST} values of **2a** (0.75 eV) and **2b** (0.62 eV). As shown in Fig. 1, the ΔE_{ST} values are tuned from 0.75 eV to 0.18 eV by manipulation of the acceptor and donor units.

3.3. Structure properties

The molecular structure of **2b** was further determined by single–crystal X–ray crystallographic analysis. The single crystal of **2b** was obtained from slow evaporation of CH_2Cl_2 solution at room temperature. The crystal data of **2b** were summarized in Table 2. As shown in Fig. 2, **2b** reveals a twisted molecular structure with a dihedral angle of 26.8° between the two phenyl rings. Crystal of **2b** exhibits edge–to–face packing of the donor (triphenyl amine) and the acceptor (benzonitrile). From the data mentioned above, the non–planarity and rigidity of the molecule is established; features which are essential in preventing the molecule from close packing and hence severe concentration quenching.

Table 2
Crystal data and structure refinement for **2b**.

Empirical formula	$C_{25}H_{18}N_2$	
CCDC No.	994818	
Formula weight	346.41	
Temperature	293(2)	
Wavelength	0.71073 Å	
Crystal system, space group	Monoclinic	
Unit cell dimensions	$a = 14.441(3)$ Å	$\alpha = 90.00°$
	$b = 8.234(16)$ Å	$\beta = 108.78(3)°$
	$c = 16.817(3)$ Å	$\gamma = 90.00°$
Volume	1893.2 (7) $Å^3$	
Z, Calculated density	4, 1.215 Mg/m^3	
Absorption coefficient	0.071 mm^{-1}	
F(000)	728	
Crystal size	0.10 × 0.20 × 0.30 mm	
Theta range for data collection	1.66–25.43°	
Limiting indices	$0 \le h <= 17$, $0 \le k <= 9$, $-20 \le l <= 19$	
Reflections collected/unique	3482/1664 [$R_{int} = 0.0911$]	
Max. and min. transmission	0.9789 and 0.9929	
Refinement method	Full-matrix least-squares on F^2	
Data/restraints/parameters	3482/0/244	
Final R indices [$I > 2$sigma(I)]	$R_1 = 0.0663$, $wR_2 = 0.1484$	
Largest diff. peak and hole	0.151 and −0.156 e $Å^{-3}$	

3.4. The UV–vis absorption spectra

Fig. 3 depicts the UV–vis absorption spectra of the four compounds in toluene. Table 2 contains a detailed listing of the UV–vis absorption spectra of these compounds in different solvents. Three major absorption bands located in the ranges of 200–250, 250–300, 300–350 nm, corresponding to the π-π^* transitions of phenyl in these compounds, and π-π^* transitions from donors (triphenyl amine or *N*–phenyl carbazole) to acceptors (benzonitrile or 2,4,6–trisphenyl–1,3,5–triazine), and intramolecular charge transfer states, respectively. From the absorption edge of the UV–vis absorption, the optical bandgap (Eg) values of the four compounds can be estimated to be 3.50 eV (**2a**), 3.20 eV (**2b**), 3.23 eV (**3a**), 3.03 eV (**3b**), which are in agreement with their calculated values. The results show that **3a** and **3b** exhibit lower Eg values than **2a** and **2b**. These may be attributed to the decrease of ICT leading to reduced π–conjugation and wide bandgap. The donor also has an effect on the Eg values. **2b** and **3b** exhibit lower Eg values than **2a** and **3a**. The results are similar to the reported sulfone–based derivatives [38,39]. Among them, changing the donor from *N*–phenylcarbazole to triphenylamine group induces a decrease of Eg values from 3.16 eV to 2.95 eV.

3.5. Electrochemical analysis

The electrochemical properties of the four compounds were studied in solution through CV using $TBAPF_6$ as the supporting electrolyte and ferrocene as the internal standard. As shown in Fig. 4, **2a**, **3a** and **3b** exhibit a reversible oxidation process, while **2b** exhibits irreversible oxidation process, which can be assigned to the oxidation of the donor units. On the basis of the onset potentials for oxidation, the HOMO energy levels of the four compounds were estimated to be −5.44 eV (**2a**), −5.39 eV (**3a**), −5.13 eV (**2b**) and −5.00 eV (**3b**). Triphenylamine substituted acceptors (**2b**, **3b**) exhibit higher HOMO energy levels than *N*–phenylcarbazole substituted acceptors (**2a**, **3a**), which are consistent with better hole-injection ability of triphenylamine [37]. From the HOMO energy levels and the Eg values, the LUMOs are estimated to be −1.93 eV, −1.94 eV, −1.97 eV and −2.16 eV for **2b**, **2a**, **3b** and **3a**, respectively.

3.6. Photoluminescence

Fig. 5 depicts the photoluminescence (PL) spectra of the four compounds in toluene. The four compounds exhibit broad and

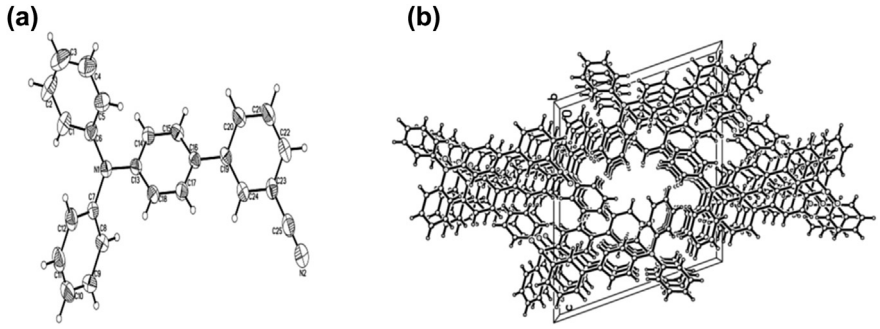

Fig. 2. (a)ORTEP diagram of **2b**. (b)Crystal packing of the compound of **2b**.

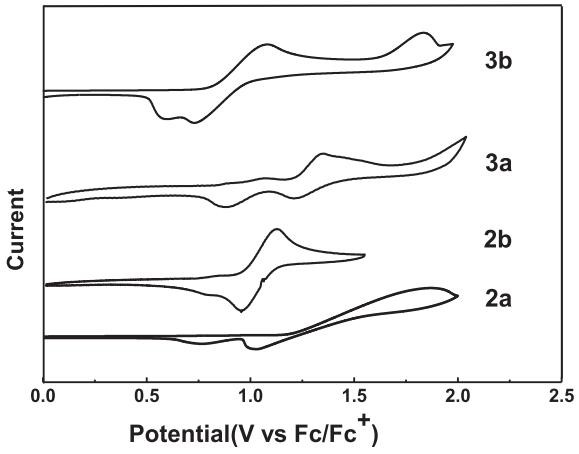

Fig. 3. Oxidation part of the CV curves of the four compounds in CH_2Cl_2 solution.

structureless emission bands in toluene with emission peaks of **2a** at 383 nm, **2b** at 407 nm, **3a** at 430 nm, and **3b** at 458 nm, respectively, which can be ascribed to the ICT. As is the case with the λ_{max} values of the four compounds, their emission maxima (λ_{fl}) are generally dependent on the acceptor group. The results show that **3a** and **3b** exhibit longer wavelengths in emission maximum than **2a** and **2b**. Changing the acceptor from benzonitrile to 2,4,6−trisphenyl−1,3,5−triazine induces a shift of the emission maximum to longer wavelengths. This may be attributed to the increase in π−conjugation. The donor group also has an effect on the emission maximum. Triphenylamine substituted acceptors (**2b** and **3b**) exhibit longer wavelengths than the corresponding *N*−phenylcarbazole substituted acceptors (**2a** and **3a**). The results are similar to the reported sulfone−based derivatives [38,39]. Among them, changing the donor from *N*−phenyl carbazole to triphenylamine group induces a shift of the emission maximum from 416 nm to 424 nm in CH_2Cl_2. The fluorescence spectra were measured in various solvents with different polarities. In the polar solvent methanol, the emission maximum of the four compounds was red−shifted to 424−501 nm. Conversely, in the nonpolar solvent hexane, the emission maximum of the four compounds was blue−shifted to 377−414 nm. As shown in Table 3, the Stokes shifts of **2b** and **3b** are larger than those of **2a** and **3a** in polar solvents attributing to the stronger ICT.

The phosphorescence spectra of the four compounds measured in a frozen 2−methyltetrahydrofuran matrix at 77 K is shown in Fig. 6. From the energy 0−0 phosphorescent emission, the triplet energy values of the four compounds are estimated to be 3.20 eV(**2a**), 3.00 eV(**2b**), 2.63 eV(**3a**), 2.64 eV(**3b**), which match the calculated results.

3.7. Delayed fluorescence

We determined the absolute fluorescence quantum yields (Φ_f) of the four compounds in toluene solution in air and the absolute delayed fluorescence quantum yields(Φ_d) in an oxygen free atmosphere (by bubbling nitrogen through the solutions for 10 min to exclude oxygen) by an integrating sphere system. The excitation wavelength used was 350 nm. As shown in Table 4, the Φ_f values of the four compounds are 0.176−0.520 in toluene solution in air. After

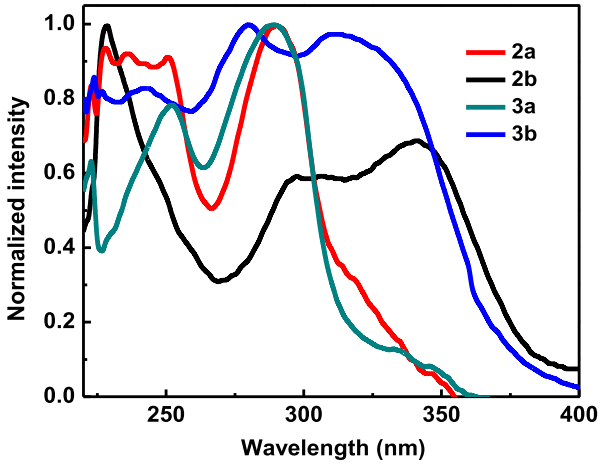

Fig. 4. Normalized UV−vis absorption spectra of the four compounds in toluene.

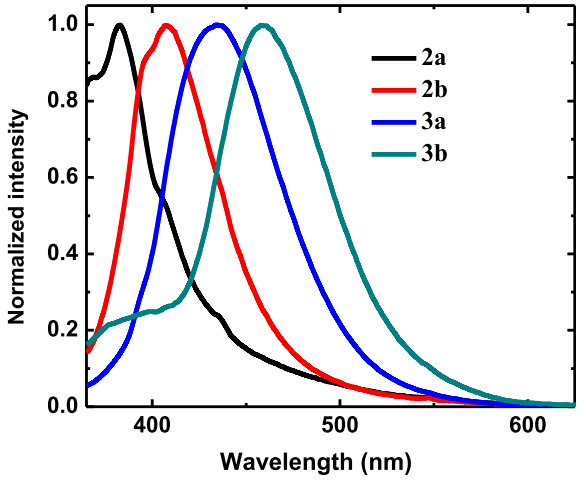

Fig. 5. Normalized photoluminescence spectra of the four compounds in toluene.

Table 3
Spectral properties of the four compounds in different solvents.

Solvent	$\Delta f(\varepsilon,n)$	**2a**			**2b**			**3a**			**3b**		
		UV	PL	$\Delta\nu$	UV	PL	$\Delta\nu$	UV	PL	$\Delta\nu$	UV	PL	$\Delta\nu$
Hexane	0	347	377	2293	341	385	3351	332	407	5550	310	414	8103
Toluene	0.013	349	383	2544	340	407	4842	330	430	7047	310	458	10,519
DCM	0.217	348	385	2762	340	445	6940	335	485	9232	310	434	9217
DMF	0.274	348	412	4464	341	460	7586	334	503	10,059	310	439	9479
MeOH	0.307	347	424	5234	340	461	7720	332	479	9244	310	501	12,298

$\Delta f(\varepsilon,n)$ corresponds to the solvent polarity parameter.
$\Delta\nu$ corresponds to the Stokes shift (in cm^{-1}) between the maxima of absorption (UV) and fluorescence emission (PL).

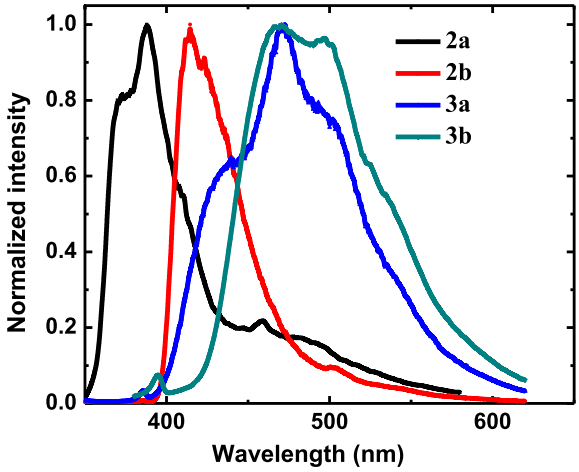

Fig. 6. The phosphorescence spectra of the four compounds measured in a frozen 2-methyltetrahydrofuran matrix at 77 K.

nitrogen bubbling, **3a** and **3b** have larger Φ_d values than **2a** and **2b**, suggesting that nitrogen bubbling suppressed the quenching of triplet states by oxygen in air and led to large Φ_d values. The results show that **3a** and **3b** can emit more delayed fluorescence and offer potential for TADF materials. The small Φ_d values of **2a** and **2b** indicate that the two compounds may not be suitable for TADF materials.

To verify the TADF behavior of **3a** and **3b** deeply, the prompt (τ_f) and delayed fluorescence lifetime (τ_d) of the two compounds were determined in toluene. In air, the solutions of **3a** and **3b** in toluene have lifetimes of 10.12 ns and 12.47 ns attributing to the prompt fluorescence. After bubbling nitrogen through the solutions for 10 min to exclude oxygen, as shown in Fig. 7, the transient photoluminescence decay characteristics of these solutions show two–component decays attributing to the prompt and delayed fluorescence. The delayed fluorescence of **3a** and **3b** in toluene, which have lifetimes of 133 μs and 166 μs, are more than four orders of magnitude longer than the prompt fluorescence.

Table 4
Cyclic voltammetry, photoluminescence properties and theoretically calculated energy levels of the four compounds.

	2a	**2b**	**3a**	**3b**
LUMO(eV)[a]	−1.31	−1.39	−1.68	−1.77
LUMO(eV)	−1.94	−1.93	−2.16	−1.97
HOMO(eV)[a]	−5.52	−5.09	−5.25	−4.92
HOMO(eV)	−5.44	−5.13	−5.39	−5.00
Eg(eV)[a]	4.21	3.70	3.57	3.15
Eg (eV)	3.50	3.20	3.23	3.03
Singlet (eV)[a]	3.76	3.36	3.19	2.82
Triplet (eV)[a]	3.01	2.74	2.82	2.64
Triplet (eV)	3.20	3.00	2.63	2.64
ΔE_{ST} (eV)[a]	0.75	0.62	0.37	0.18
Φ_f	0.216	0.520	0.178	0.176
Φ_d	0.041	0.032	0.142	0.442
τ_f (ns)			10.12	12.47
τ_d (μs)[b]			133	166
k_f (10^7 S^{-1})			1.76	1.41
k_d (10^3 S^{-1})			1.07	2.66
ΔE_{ST} (eV)			0.22	0.19
Singlet (eV)[c]			2.77	2.60
Triplet (eV)[c]			2.53	2.42
ΔE_{ST} (eV)[c]			0.24	0.18

[a] Theoretically calculated energy levels of the four compounds.
[b] In an oxygen free atmosphere (by bubbling nitrogen through the solution for 10 min to exclude oxygen).
[c] Singlet energy levels are estimated from the photoluminescence (PL) spectra in film at 77 K. Triplet energy levels are estimated from the phosphorescence spectra with 100 μs delay in film at 77 K.

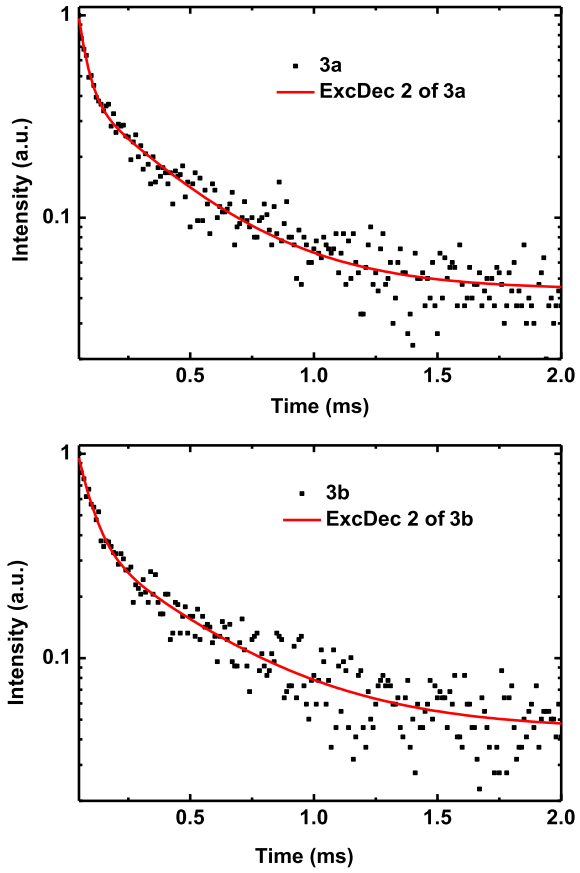

Fig. 7. Emission decay curves and fitting curves of **3a** and **3b** in an oxygen free atmosphere (by bubbling nitrogen through the solution for 10 min to exclude oxygen) in toluene at 300 K. The value of Adj. R-Square (>0.97) is used to ensure the quality of the fit.

According to the literature [12], ΔE_{ST} can be calculated using equations (1)–(4):

$$k_f = \Phi_f / \tau_f \quad (1)$$

$$k_d = \Phi_d / \tau_d \quad (2)$$

$$K = 1/3\exp(-\Delta E_{ST}/RT) \quad (3)$$

$$k_d = k_f K \quad (4)$$

where k_f, k_d, R, T and 1/3 donate the rate constants of fluorescence, the rate constants of TADF, the idea gas cnstant, abusolute temperature (300 K), and the ratio of the degeneracies of singlet state to triplet state, respectively [12].

From equations (1)–(4), the ΔE_{ST} of **3a** and **3b** are estimated to be 0.19 eV and 0.22 eV as shown in Table 4, which are consistent with the TD–DFT results.

To obtain the ΔE_{ST} values, we examined the time-resolved fluorescence and phosphorescence spectra of **3a** and **3b** in solid films with 100 μs delay at 77 K. As shown in Fig. 8, **3a** and **3b** exhibit unstructured phosphorescent emission spectra with peaks at 491 nm and 512 nm, their triplet energy values are estimated to be 2.53 eV and 2.42 eV. From the fluorescence emission spectra of **3a** and **3b** with peaks at 447 nm and 477 nm, their singlet energy values are obtained to be 2.77 eV and 2.60 eV. Thus, the ΔE_{ST} values of **3a** and **3b** are estimated to 0.24 eV and 0.18 eV, respectively, which are in good agreement with the calculated values based on the prompt and delayed fluorescence data.

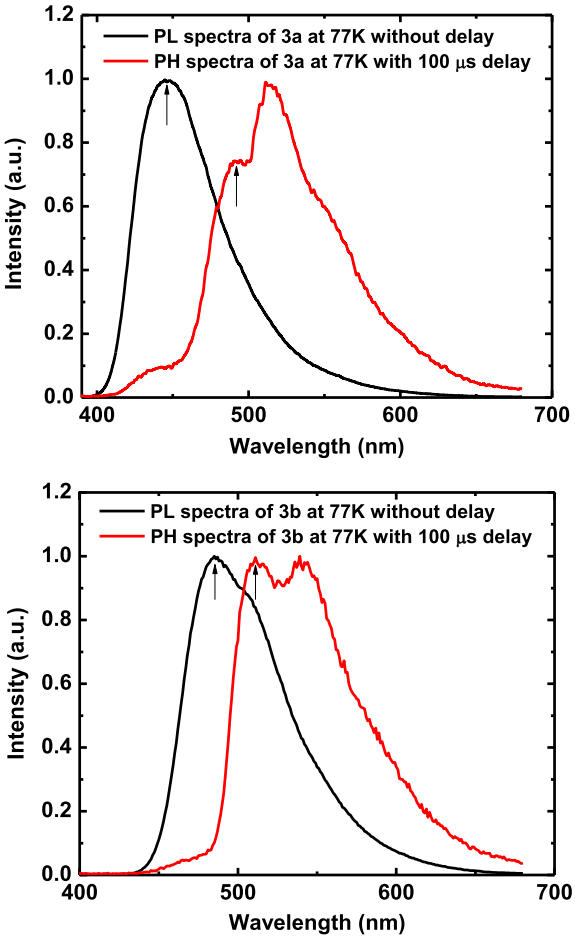

Fig. 8. The time-resolved photoluminescence (PL) and phosphorescence (PH) spectra of **3a** and **3b** in solid films with 100 μs delay at 77 K.

4. Conclusions

In summary, we have designed and synthesized a series of ambipolar materials based on donors substituted benzonitrile and 2,4,6–trisphenyl–1,3,5–triazine. The photo–physical properties of the four compounds have been systematically investigated by TD–DFT calculations, UV–vis, fluorescence spectroscopic measurements, and CV. *N*–phenyl carbazole and triphenylamine functionalized tris(aryl)triazines are potent TADF materials with small ΔE_{ST} values of 0.24 eV and 0.18 eV. The ΔE_{ST} values based on the time-resolved fluorescence and phosphorescence spectra are in good agreement with the calculated values based on the prompt and delayed fluorescence data. In all, we present a novel strategy for tuning the ΔE_{ST} values in ambipolar systems for TADF by manipulation the constitution of acceptor and donor units.

Acknowledgments

This work was supported by the National Natural Science Foundation of China (Grant No.51103023 and 21173042), the National Basic Research Program of China (Grant No.2013CB932900), the Research Fund for Graduate Innovation Project of Jiangsu Province (No.CXZZ13_0090), the Science and technology support program (industry) project of jiangsu province (BE 2013118), the Natural Science Foundation of the Jiangsu Higher Education Institutions of China (No.14KJB150003) and Jiangsu Provincial Natural Science Foundation for Youths (No. BK20130749).

References

[1] Baldo MA, O'Brien DF, You Y, Shoustikov A, Sibley S, Thompson ME, et al. Highly efficient phosphorescent emission from organic electroluminescent devices. Nature 1998;395:151–4.
[2] Reineke S, Lindner F, Schwartz G, Seidler N, Walzer K, Lüeesem B, et al. White organic light–emitting diodes with fluorescent tube efficiency. Nature 2009;459:234–9.
[3] Xiao LX, Chen ZJ, Qu B, Luo JX, Kong S, Gong QH, et al. Recent progresses on materials for electrophosphorescent organic light–emitting devices. Adv Mater 2011;23:926–52.
[4] Tao YT, Yang CL, Qin JG. Organic host materials for phosphorescent organic light–emitting diodes. Chem Soc Rev 2011;40:2943–70.
[5] Kim K, Moon C, Lee J, Kim S, Kim J. Highly efficient organic light–emitting diodes with phosphorescent emitters having high quantum yield and horizontal orientation of transition dipole moments. Adv Mater 2014;26:3844–7.
[6] Lee CW, Lee JY. Above 30% external quantum efficiency in blue phosphorescent organic light–emitting diodes using pyrido[2,3–*d*]indole derivatives as host materials. Adv Mater 2013;25:5450–4.
[7] Hashimoto M, Igawa S, Yashima M, Kawata I, Hoshino M, Osawa M. Highly efficient green organic light–emitting diodes containing luminescent three–coordinate copper(I) complexes. J Am Chem Soc 2011;133:10348–51.
[8] Zhang Q, Komino T, Huang S, Matsunami S, Goushi K, Adachi C. Triplet exciton confinement in green organic light–emitting diodes containing luminescent charge–transfer Cu(I) complexes. Adv Funct Mater 2012;22:2327–36.
[9] Uoyama H, Goushi K, Shizu K, Nomura H, Adachi C. Highly efficient organic light–emitting diodes from delayed fluorescence. Nature 2012;492:234–40.
[10] Nakanotani H, Higuchi T, Furukawa T, Masui K, Morimoto K, Numata M, et al. High–efficiency organic light–emitting diodes with fluorescent emitters. Nat Commun 2014;5:4016–22.
[11] Zhang D, Duan L, Li C, Li Y, Li H, Zhang D, et al. High–efficiency fluorescent organic light–emitting devices using sensitizing hosts with a small single–t–triplet exchange energy. Adv Mater 2014;26:5050–5.
[12] Zhang Q, Li B, Huang S, Nomura H, Tanaka H, Adachi C. Efficient blue organic light–emitting diodes employing thermally activated delayed fluorescence. Nat Photon 2014;8:326–32.
[13] Tao Y, Yuan K, Chen T, Xu P, Li H, Chen R, et al. Thermally activated delayed fluorescence materials towards the breakthrough of organoelectronics. Adv Mater 2014;26:7931–58.
[14] Li B, Nomura H, Miyazaki H, Zhang Q, Yoshida K, Suzuma Y, et al. Dicarbazolyldicyanobenzenes as thermally activated delayed fluorescence emitters:

effect of substitution position on photo luminescent and electroluminescent properties. Chem Lett 2014;43:319–21.
[15] Cho YJ, Yook KS, Lee JY. High efficiency in a solution–processed thermally activated delayed–fluorescence device using a delayed–fluorescence emitting material with improved solubility. Adv Mater 2014;26:6642–6.
[16] Zhang D, Duan L, Zhang D, Qiao J, Dong G, Wang L, et al. Extremely low driving voltage electrophosphorescent green organic light–emitting diodes based on a host material with small singlet–triplet exchange energy without p– or n–doping layer. Org Electron 2013;1:260–6.
[17] Zhang D, Duan L, Li Y, Li H, Bin Z, Zhang D, et al. Towards high efficiency and low roll–off orange electrophosphorescent devices by fine tuning singlet and triplet energies of bipolar hosts based on indolocarbazole/1, 3, 5–triazine hybrids. Adv Funct Mater 2014;23:3551–61.
[18] Sato K, Shizu K, Yoshimura K, Kawada A, Miyazaki H, Adachi C. Organic luminescent molecule with energetically equivalent singlet and triplet excited states for organic light–emitting diodes. Phys Rev Lett 2013;110:247401–5.
[19] Endo A, Sato K, Yoshimura K, Kai T, Kawada A, Miyazaki H, et al. Efficient up–conversion of triplet excitons into a singlet state and its application for organic light emitting diodes. Appl Phys Lett 2011;98:83302.
[20] Serevicius T, Nakagawa T, Kuo MC, Cheng SH, Wong KT, Chang CH, et al. Enhanced electroluminescence based on thermally activated delayed fluorescence from a carbazole–triazine derivative. Phys Chem Chem Phys 2013;15:15850–5.
[21] Tanaka H, Shizu K, Miyazaki H, Adachi C. Efficient green thermally activated delayed fluorescence (TADF) from a phenoxazine–triphenyltriazine (PXZ–TRZ) derivative. Chem Commun 2012;48:11392–4.
[22] Mayr C, Lee SY, Schmidt TD, Yasuda T, Adachi C, Brütting W. Efficiency enhancement of organic light–emitting diodes incorporating a highly oriented thermally activated delayed fluorescence emitter. Adv Funct Mater 2014;24:5232–9.
[23] Lee SY, Yasuda T, Nomura H, Adachi C. High–efficiency organic light–emitting diodes utilizing thermally activated delayed fluorescence from triazine–based donor– hybrid molecules. Appl Phys Lett 2012;101:93306.
[24] Komino T, Tanaka H, Adachi C. Selectively controlled orientational order in linear–shaped thermally activated delayed fluorescent dopants. Chem Mater 2014;26:3665–71.
[25] Tanaka H, Shizu K, Nakanotani H, Adachi C. Twisted intramolecular charge transfer state for long–wavelength thermally activated delayed fluorescence. Chem Mater 2013;25:3766–71.
[26] Zhang Q, Li J, Shizu K, Huang S, Hirata S, Miyazaki H, et al. Design of efficient thermally activated delayed fluorescence materials for pure blue organic light emitting diodes. J Am Chem Soc 2012;134:14706–9.
[27] Wu S, Aonuma M, Zhang Q, Huang S, Nakagawa T, Kuwabara K, et al. High–efficiency deep–blue organic light–emitting diodes based on a thermally activated delayed fluorescence emitter. J Mater Chem C 2014;2:421–4.
[28] Huang B, Qi Q, Jiang W, Tang J, Liu Y, Fan W, et al. Thermally activated delayed fluorescence materials based on 3,6–di–*tert*–butyl–9–((phenylsulfonyl) phenyl)–9*H*–carbazoles. Dyes Pigments 2014;111:135–44.
[29] Lee SY, Yasuda T, Yang YS, Zhang Q, Adachi C. Luminous butterflies: efficient exciton harvesting by benzophenone derivatives for full–color delayed fluorescence OLEDs. Angew Chem Int Ed 2014;53:6402–6.
[30] Li J, Nakagawa T, MacDonald J, Zhang Q, Nomura H, Miyazaki H, et al. Highly efficient organic light–Emitting diode based on a hidden thermally activated delayed fluorescence channel in a heptazine derivative. Adv Mater 2013;25:3319–23.
[31] Lee J, Shizu K, Tanka H, Nomura H, Yasuda T, Adachi C. Oxadiazole– and triazole–based highly–efficient thermally activated delayed fluorescence emitters for organic light–emitting diodes. J Mater Chem C 2013;1:4599–604.
[32] Huang B, Jiang W, Tang J, Ban X, Zhu R, Xu H, et al. A novel, bipolar host based on triazine for efficient solution–processed single–layer green phosphorescent organic light–emitting diodes. Dyes Pigments 2014;101:9–14.
[33] Gaussian 09 (Revision A.01). Wallingford, CT: Gaussian, Inc; 2009.
[34] Cho I, Kim SH, Kim JH, Park S, Park SY. Highly efficient and stable deep–blue emitting anthracene–derived molecular glass for versatile types of non–doped OLED applications. J Mater Chem 2012;22:123–9.
[35] Im Y, Lee JY. Above 20% external quantum efficiency in thermally activated delayed fluorescence device using furodipyridine–type host materials. Chem Mater 2014;26:1413–9.
[36] Su SJ, Sasabe H, Pu YJ, Nakayama K, Kido J. Tuning energy levels of electron–transport materials by nitrogen orientation for electrophosphorescent devices with an 'ideal' operating volta. Adv Mater 2010;22:3311–6.
[37] Wang H, Xie L, Peng Q, Meng L, Wang Y, Yi Y, et al. Novel thermally activated delayed fluorescence materials–thioxanthone derivatives and their applications for highly efficient OLEDs. Adv Mater 2014;26:5198–204.
[38] Zheng CJ, Wang J, Ye J, Lo MF, Liu XK, Fung MK, et al. Novel efficient blue fluorophors with small singlet–triplet splitting: hosts for highly efficient fluorescence and phosphorescence hybrid WOLEDs with simplified structure. Adv Mater 2013;25:2205–11.
[39] Ye J, Chen Z, Fung MK, Zheng C, Ou X, Zhang X, et al. Carbazole/sulfone hybrid D–π–A–structured bipolar fluorophores for high–efficiency blue–violet electroluminescence. Chem Mater 2013;25:2630–7.